42nd AIAA Aerospace Sciences Meeting and Exhibit
5 - 8 January 2004, Reno, Nevada

AIAA 2004-138

Lean Blowout Detection in a Single Nozzle Swirl Cup Combustor

S. Nair[*], T. M. Muruganandam[*], R. Olsen[†], A. Meyers[‡], J. Seitzman[§], B. Zinn[**], T. Lieuwen[††]
School of Aerospace Engineering
Georgia Institute of Technology, Atlanta, GA 30332-0150

T. Held, H. Mongia
General Electric Aircraft Engines, Cincinnati, OH 45215

Abstract

This paper describes work to develop practical, fast diagnostic techniques that can be used to monitor the proximity of a combustor to blowoff using measurements of the flame's acoustic and chemiluminescence signature. Data was acquired from a commercial single nozzle, swirl cup combustor fueled with Jet-A. High-speed flame images were obtained and analyzed in conjunction with simultaneous acoustic and optic data. These analyses revealed changes in the low frequency acoustic spectrum and increased presence of time-localized and intermittent events in both acoustic and optic data as the combustor approached blowoff. Based upon these observations, spectral, wavelet and thresholding signal-processing schemes were developed for detecting blowout precursors with varying levels of time response, sensitivity and robustness.

Introduction

Combustor blowout is a serious concern in modern land-based and aero engine combustors, particularly in aircraft engines where the combustion process is ultimately the source of the vehicle's thrust. In military and commercial aircraft engines, blowoff avoidance during sudden changes in throttle setting is a major design consideration. During rapid decelerations, the fuel flow rate can be reduced very quickly, while the slower airflow transient rate is controlled by the rotational inertia of the compressor[1]. In addition, the low temperatures and pressures at high altitudes make relight after a blowoff event very difficult. Blowout is also a major concern in land-based power generating industrial systems, where the engines are required to operate economically and reliably over long periods with minimal shutdown time. Emission legislations have motivated current lean, premixed combustor designs, enhancing risk of blowoff. Blowoff events may require lengthy (and therefore expensive) system shutdowns and restarts, which increases maintenance costs and reduces engine life and availability.

Currently, blowoff is avoided by operating the combustor with a wide safety margin from the somewhat uncertain stability limit (i.e., at higher equivalence ratio). Reduction in this margin can potentially result in lower pollutant emissions and enable faster engine transients. The ability to sense blowoff precursors can therefore provide significant payoffs in engine reliability and operability, in enabling optimal performance over extended periods of time, in reducing maintenance costs and extending engine life. In prior studies, we have demonstrated that the blowoff stability margin can be monitored through suitable analyses of the flame's acoustic and optical signature[2-5]. This work is primarily carried out in a gaseous fueled, premixed combustor that closely resembles current land based gas turbine designs. This paper extends this work to a non-premixed, liquid-fueled combustor using actual aircraft engine hardware.

Background

In practical combustors, sustained combustion occurs over a parametric space, often referred to as the region of static stability of the combustion process. The term "static stability" is used to distinguish blowout from "dynamic stability", which usually refers to self-excited, combustion driven oscillations that involve chemical energy being fed into acoustic oscillations. The loss of static stability is referred to as blowout. A stable flame can be sustained in the combustor only

[*] Graduate Research Assistant, AIAA Student Member
[†] Undergraduate Research Assistant, AIAA Student Member
[‡] Research Engineer I, AIAA Member
[§] Associate professor, AIAA Associate Fellow
[**] Regents Professor, AIAA Fellow
[††] Assistant Professor, AIAA Member

over a certain range of fuel/air ratios, see **Figure 1**. The figure plots the typical qualitative dependence of the range of fuel/air ratios over which stable combustion can occur upon a combustor loading parameter[6]. This loading parameter increases with combustor flow velocities (i.e., reduced residence time) or at lower ambient temperatures and densities (i.e., longer chemical times).

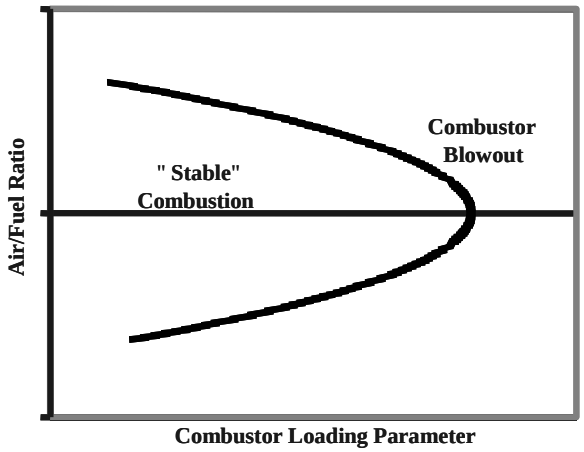

Figure 1 Stability map showing regions where sustainable combustion is possible[6].

This work is motivated by observations that the combustion process exhibits enhanced unsteadiness while transitioning between the static stability and blowoff[7-9]. However, the primary focus of the existing literature on the subject is devoted to predicting the blowout limits of a given system as a function of such parameters as equivalence ratio, air temperature, or pressure[10-14]. Little work has been done to characterize the combustion processes as it transitions from static stability to blowoff. The objective of this work is to characterize the acoustic and chemiluminescence emissions of flames under such circumstances. This objective is motivated by the desire to develop practical, non-intrusive, and fast diagnostic techniques that can be used to detect the onset of blowout in realistic combustion devices.

Acoustic emissions provide a useful diagnostic into transient flame holding events because they are proportional to the temporal rate of change of heat release. Fundamentally, combustion noise is generated by the unsteady expansion of reacting gases in turbulent flames that excite acoustic waves over a broad range of frequencies (typically between ~10 Hz – 25 kHz). Thus, acoustic measurements can be used to detect either global changes in heat release rate or fluctuations in heat release at certain time scales by measuring their acoustic emissions in corresponding frequency bands[15].

Spontaneous chemiluminescence emissions also provide useful diagnostics into unsteady combustion reaction characteristics. This radiation is from high-energy states of molecules (typically electronically excited states) that are produced by chemical reactions. Once produced, the excited molecules will transfer to lower energy states, in part by emitting light, which is known as chemiluminescence. Since the intensity of emission is proportional, in part, to the chemical production rate of the particular molecule, the chemiluminescence intensity can be related to (specific) chemical reaction rates.[16] For this reason, chemi-luminescence has been used previously as a rough measure of reaction rate and heat release rate.[17-23] Thus, chemiluminescence can provide information on the presence and strength of the combustion process in a specific region of the combustor, making it well suited for health monitoring and diagnostics.

Instrumentation and Experimental Facility

Experiments were performed on an atmospheric pressure, single cup swirl combustor, illustrated in **Figure 2**, which is a part of a commercial flight engine used on a variety of Boeing and Airbus platforms. Only the front end of the combustor was retained. The remainder of the combustor was built around this hardware to facilitate diagnostics. The test-section sidewalls are made of quartz glass to facilitate detection of UV radiation and high-speed imaging. The top and bottom walls consist of thermal-barrier coated (TBC) metal plates that were machined out in an arc to simulate the annular shape of the actual hardware. In the same way, the windows are set in at angles, so that the resulting chamber mimics a single nozzle in an annular combustor.

Non-vitiated, preheated air is supplied to the swirl cup from plenum chamber. Air enters the combustor through counter-rotating swirlers, while the fuel is injected through a centrally located fuel nozzle. This is followed by a small annular passage leading to the test section. Because the fuel flow rates are substantially lower than in the actual engine (about $1/30^{th}$ at full power), the standard fuel nozzle was replaced with a pressure-swirl atomizer. Aviation grade, Jet A fuel, essentially a kerosene-based fuel with additional corrosive inhibitors, was used for all tests. The reactive mixture was ignited with a spark plug, recessed within the top flange, as shown in **Figure 2**.

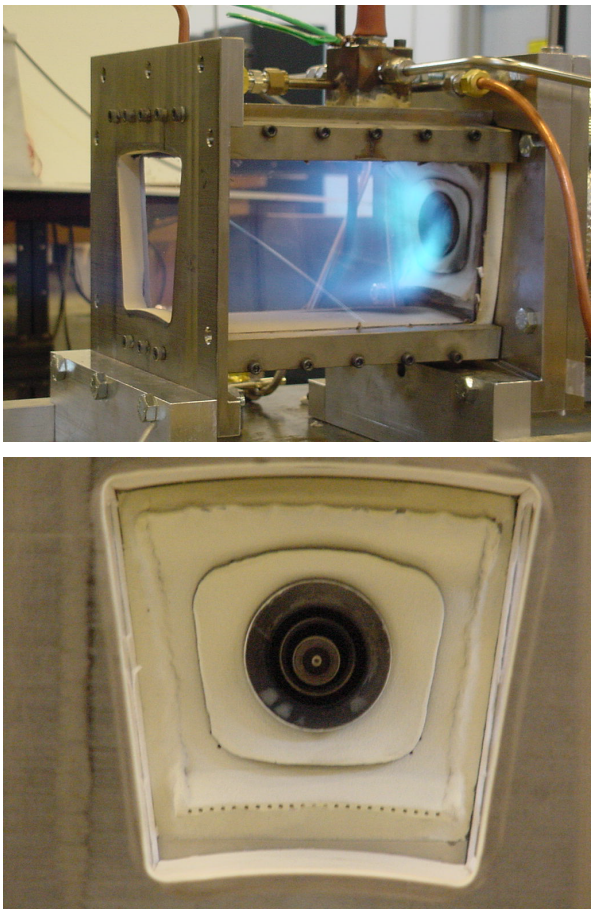

Figure 2 Photograph (side-view and front-view) of the swirl cup combustor.

Acoustic oscillations were measured with calibrated, Bruel and Kjaer type 4939 condenser microphones that have a flat frequency response up to 40 kHz. Their output was low pass filtered at 5 kHz and then fed into a 12 bit, 16-channel National Instruments A/D board. A total of 65,536 (i.e., 2^{16} points) data points were obtained at a sampling frequency of 10 kHz. Chemiluminescence measurements were made using a 365μm diameter fused silica optical fiber. The fiber has an acceptance cone half angle of about 12^{o}. This system also includes an OH interference filter, centered at 308 nm, with a 10 nm spectral width. The collected light is imaged onto the detector in a miniature, metal package PMT (Hamamatsu H5784-04). This PMT has a built-in amplifier (bandwidth of 20 kHz) to convert the current to voltage and operates from a 12VDC source. The field of view for the optical system is shown in **Figure 3**.

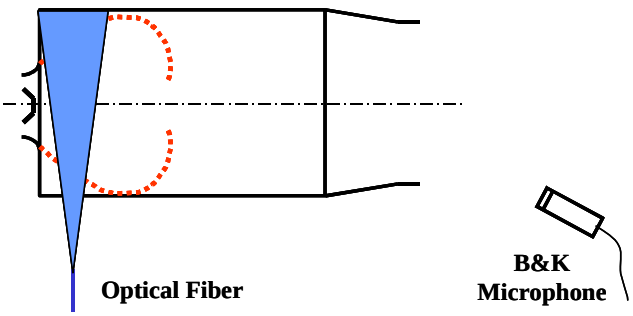

Figure 3 Schematic of the swirl burner used, the location of the fiber, microphone and the chemiluminescence collection volume.

High-speed images of the flame under stable and near blow-off conditions were obtained in order to better understand the phenomenology of the flame blow-off process, and hence, improve capabilities for interpreting the acoustic and optic signature. A high-speed intensified CCD camera (Kodak Ektapro 239×192 full frame resolution) was used with a UV Nikkor camera lens to image the flames. Images were captured with an intensifier gating time of 150 μsec at 1000 frames/second. All images were obtained with a UV spectral filter.

A thermocouple was used to monitor the change in the temperature of the combustor wall.

Blowoff Phenomenology

In this section, we describe the phenomenology of the flame blow-off process. High-speed images are presented in conjunction with simultaneous acoustic and optic data to aid the development of data-analysis schemes described in the next section. The combustor's proximity to blow-off was controlled by the equivalence ratio, which was adjusted via the overall fuel flow rate while keeping the overall airflow fixed. The overall equivalence ratio (i.e., calculated using all the air coming through the front end) was varied between 0.3 and 0.9. The blow-off equivalence ratio for this combustor was just below 0.35 for the flow conditions used. **Figure 4** and **Figure 5** plots a sequence of images (turned anti-clockwise) for a stable flame at an equivalence ratio normalized by its value at blowoff, ϕ/ϕ_{LBO} of 1.2 and for a flame close to blowout, ϕ/ϕ_{LBO} of 1.02. In the $\phi/\phi_{LBO} = 1.2$ case, there is always a well-defined combustion region. For the flames close to blowout, a near flame loss event is occasionally seen. In the latter case, the combustor initially has a spatially distributed combustion zone. Then, the flame begins to disappear from the field of view and there is an almost complete loss of flame. Then, the radiation signal re-

appears, suggesting re-ignition of the unburned fuel. This process then repeats itself. These extinction and re-ignition events span a period of several milliseconds, and occur randomly in time (with no fixed frequency) prior to blowout. As the lean blowout limit is approached, the frequency and duration of these events increase.

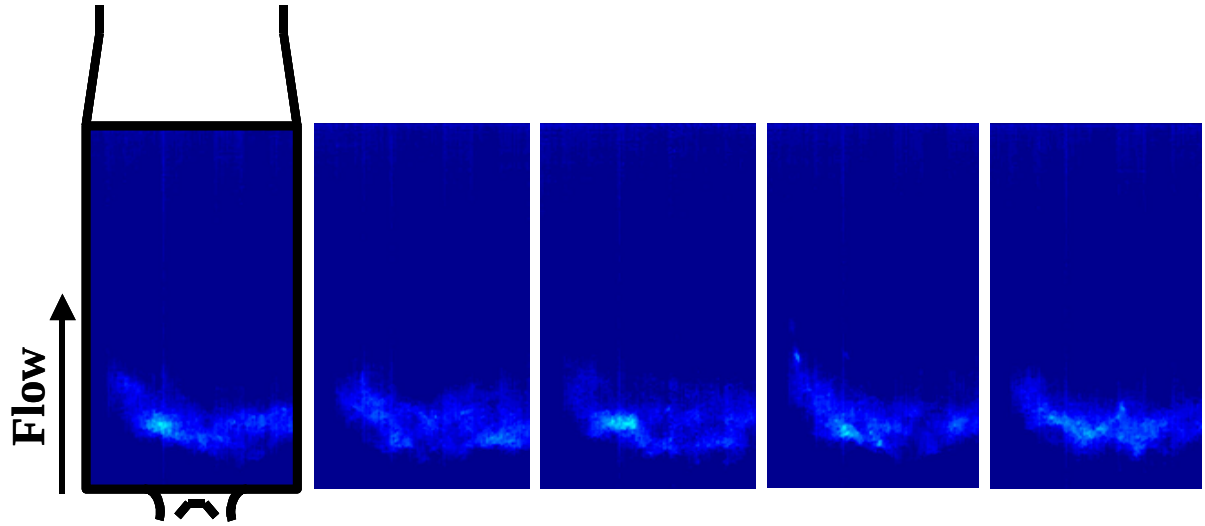

Figure 4 High-speed camera images taken at a 4 msec interval of stable flames at a ϕ/ϕ_{LBO} = 1.2.

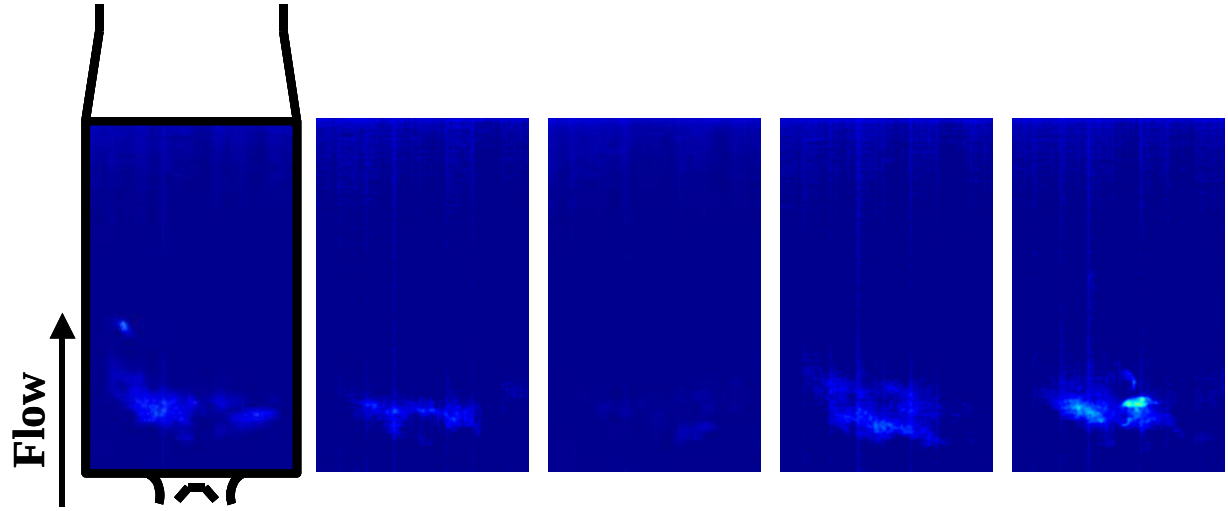

Figure 5 High-speed camera images taken at a 4 msec interval of flames close to blowout at a ϕ/ϕ_{LBO} = 1.02.

Figure 6 plots typical measured time dependencies of the acoustic pressure at several normalized equivalence ratios, ϕ/ϕ_{LBO}=1.56 and 1.03. Note the reduction in RMS pressure levels with equivalence ratio, due to the reduced heat release at the lower fuel flow rates. Near blowout, short time duration, high amplitude bursts are observed. These bursts coincide with the occurrence of the flame loss and re-ignition events described in the high-speed video images.

Figure 7 plots typical measured time dependencies of the OH^* chemiluminescence at normalized equivalence ratios, ϕ/ϕ_{LBO}=1.37 and 1.02. The average intensity decreased with equivalence ratio as expected, due to reduced heat release. More importantly, as the combustor is operated closer to its blowout limit, the OH chemiluminescence occasionally

drops to a "near" zero value, indicating the occurrence of the short duration, extinction events.

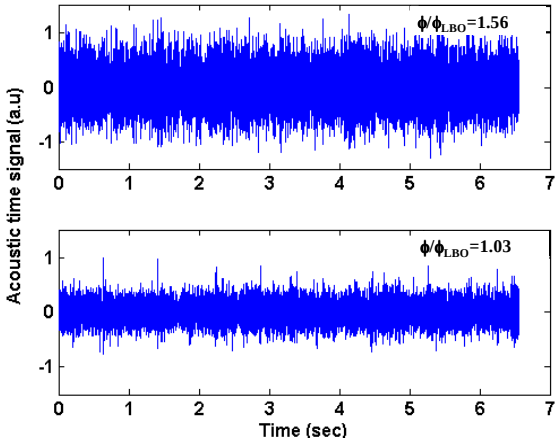

Figure 6 Acoustic signal from the burner for ϕ/ϕ_{LBO} = 1.56 (stable case) and 1.03 (close to blowout).

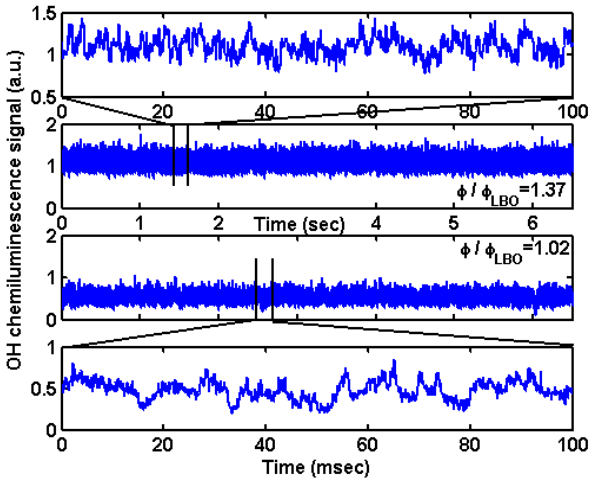

Figure 7 OH* chemiluminescence signal from the burner for ϕ/ϕ_{LBO} = 1.37 (stable case) and 1.02 (close to blowout).

Signal Analysis Strategies

Developing data analysis schemes with maximum sensitivity, speed and robustness requires a thorough understanding of the flame characteristics prior to blowout. The high-speed flame images obtained and analyzed in conjunction with simultaneous acoustic and optic data were used to aid the development of such schemes. These analyses revealed increases in number and duration of time-localized bursts (or "events") in the signal as the flame approached blowout. A straightforward approach to detect such time-localized surges in the signal is to use thresholding or maximum/mean ratio analysis. The basic idea behind this approach is to count the number of times the instantaneous signal level crosses a threshold value (e.g. large bursts during extinction or re-ignition), usually defined as some multiple of the signal's mean or R.M.S. Because the acoustic signal is a spatially integrated measure of the unsteady heat release over the entire flame, very pronounced changes in the heat release in a localized region of the flame may not be very evident in the overall signal. As such, we found thresholding techniques to be most useful when performed after pre-processing or filtering of the acoustic data. In contrast, because optical measurements can be focused upon localized spatial regions, thresholding of the raw signal can be a very sensitive blowoff indicator.

Conventional spectral or wavelet-based time-frequency analysis can be employed for filtering the acoustic signal for finding changes in signal characteristics or extracting features in the signal. Conventional power spectra can be estimated by dividing the raw data record into 32 ensembles. Power spectral densities (PSD) is obtained for each ensemble and then averaged. The primary limitation of this approach is its insensitivity to time-localized events. This shortcoming can be circumvented to some extent (within the limitations of the time-frequency uncertainty principle[24]) with time-frequency data analysis using the wavelet transform. The wavelet transform is defined as:

$$f_{\psi}(t) = \int_{t'} W((t' - t)/\psi)p(t)dt' \quad (1)$$

where p(t) is the raw time series data, ψ is a scaling parameter, and W(t) is the wavelet basis function. For example, the "Mexican Hat" is a popular wavelet whose functional dependence is given by:

$$W_1(t) = \frac{2}{\sqrt{3}}\pi^{-1/4}(1-t^2)e^{-t^2/2} \quad (2)$$

The wavelet operation is a generalization of a moving Fourier transform, which can be recovered by replacing the kernel W(t) by the complex exponential, e^{-it} In this case, the parameter ψ is the inverse of the frequency, $\psi = 1/f$. In general, note that this convolution operation depends upon two parameters: translation, t, and dilatation, ψ. Its basic operation is to determine how much the pressure in some localized interval around time, t, "looks like" the wavelet basis function W(t) at the scale, ψ. Thus, it can be used for detection of features with certain prescribed characteristics and time scales. This is useful for cases

where we know *a priori* the temporal characteristics of the blowout precursor. By defining a wavelet with these characteristics, the wavelet operation can be used to extract such precursors from noisy data.

Consider the following issues and tradeoffs associated with three key performance metrics of a blowout detection scheme:

1. *Time response* is a critical feature if it is to be used in systems where blowout is to be avoided during fast transients. For example, a time response of less than one second is required in a high performance military engine, which must remain stable during very rapid throttle increases or decreases. A key tradeoff exists between fast time response and robustness, as false alarms can be minimized and confidence in blowout proximity can be maximized by increasing the amount of data considered in estimating blowoff proximity.

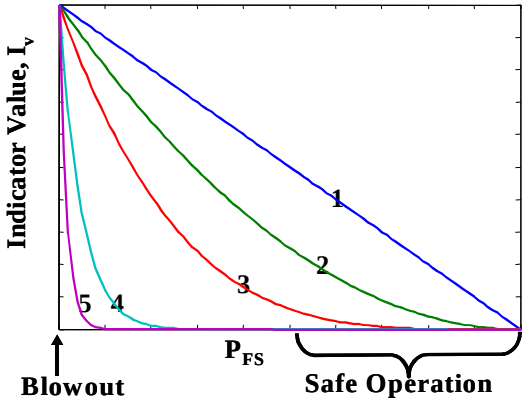

Figure 8 Dependence of a quantitative blowout indicator, I_V, upon a parameter affecting flame stability, P_{FS}.

2. *Sensitivity*: Consider the dependence of some quantitative blowout indicator, I_v (e.g., number of signal threshold crossings) upon a parameter that affects the flame stability, P_{FS} (e.g. equivalence ratio, pilot level, mean pressure), see **Figure 8**. First, it is critical that the ratio of I_v near blowout to when the flame is well stabilized should be very large relative to inherent noise or uncertainty, i.e., $I_{v,\ blowout}/I_{v,\ \text{“safe”}} >> 1$. Second, the indicator value should have a one-to-one correspondence with blowout proximity; i.e., it should increase monotonically as blowout is approached. All five curves shown in **Figure 8** satisfy this requirement. The third issue related to sensitivity is the functional dependence of I_v upon P_{FS}. Referring to **Figure 8**, it seems preferable that the curves have a change in gradient, dI_v/dP_{FS} near blowout, such as is manifested in curves 3, 4, and 5. In contrast, the dependence of I_v upon P_{FS} in curve 1 is not ideal as I_v achieves significant nonzero values even when the system is still very “safe” and dI_v/dP_{FS} has a constant value that is independent of P_{FS}. Fourth, the optimal P_{FS} value where the dI_v/dP_{FS} change occurs is important. Preferably, it should not be overly conservative and occur in regions that are still quite safe, e.g., curve 2. However, it should not also occur too close to the point of blowoff, such as curve 5.

The shape of the I_v vs. P_{FS} curve can be manipulated to some extent through suitable changes in signal processing parameters, such as threshold levels. There is often a tradeoff in these first and fourth requirements as signal processing parameters that result in larger $I_{v,\ blowout}/I_{v,\ \text{“safe”}}$ values generally result in P_{FS} vs. I_v curves resembling curves 1 or 2. In contrast, the more ideal curves 3 or 4 often have substantially lower $I_{v,blowout}/I_{v,\ \text{“safe”}}$ values.

3. *Robustness*: As mentioned above, the signal analysis approach must also be robust to inherent levels of noise and uncertainty. Obviously, robustness of a particular approach is enhanced by having a large number of ensembles of data in order to average out noise. In addition, I_v values at a fixed P_{FS} must be relatively insensitive to small deviations in signal processing parameters (e.g. threshold level) and system aging.

Spectral and Wavelet Analysis

This section describes the Fourier analysis of the acoustic data from the burner. The combustion noise spectra from the burner at two different normalized equivalence ratios, $\phi/\phi_{LBO} = 1.56$ and 1.03 are plotted in **Figure 9**. Each curve has been normalized to have the same total acoustic power in order to correct for the different fuel flow rates in each case. As indicated in **Figure 9**, there is an increase in power below 200 Hz spectral regime under these near flameout conditions.

Figure 10 plots the dependence of the acoustic power in the 10-100 Hz frequency range normalized by the total power in the acoustic signal against normalized equivalence ratios. The power in the spectral band increases by a factor of nearly 3 near blowout. Referring to **Figure 9**, it can be seen that the relative sensitivity of this ratio is comparatively constant below about 100 Hz, but it rapidly diminishes at higher frequencies.

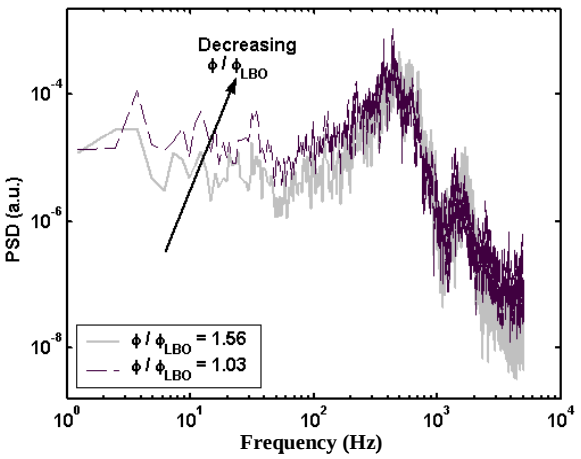

Figure 9 Normalized acoustic spectra of the combustor for ϕ/ϕ_{LBO}= 1.56 and 1.03.

The acoustic data from this combustor was also examined using wavelet analysis. In order to increase sensitivity, "customized" wavelets4 were chosen which resembled the actual acoustic events close to blowout. The temporal characteristics of these events were determined from simultaneous analysis of OH^* chemiluminescence and the acoustic signal. **Figure 11** shows a plot of acoustic and optical data at an equivalence ratio close to blowoff. A detail of these data is also shown in the right half of **Figure 11**. The large dips in the optical signal suggest local temporary flame loss. A coincident feature is also evident in the acoustic signal, which resembles the derivative of the OH^* signal, as expected. The following customized wavelet was generated, whose waveform is similar to the acoustic signature during these events:

$$W_2(t) = -\frac{d}{dt}(e^{-t^2/2}) \qquad (5)$$

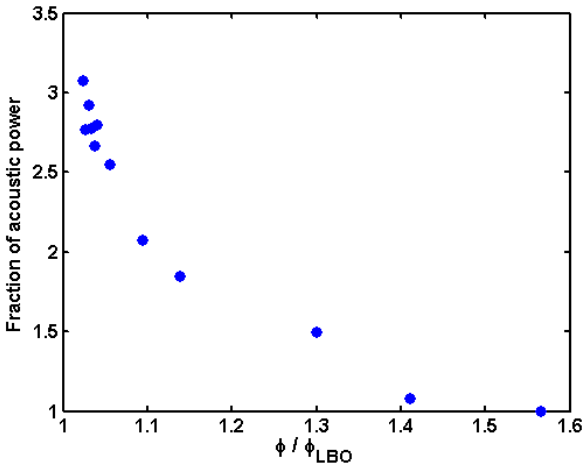

Figure 10 Dependence of the normalized acoustic power in the 10-100 Hz frequency band upon ϕ/ϕ_{LBO}.

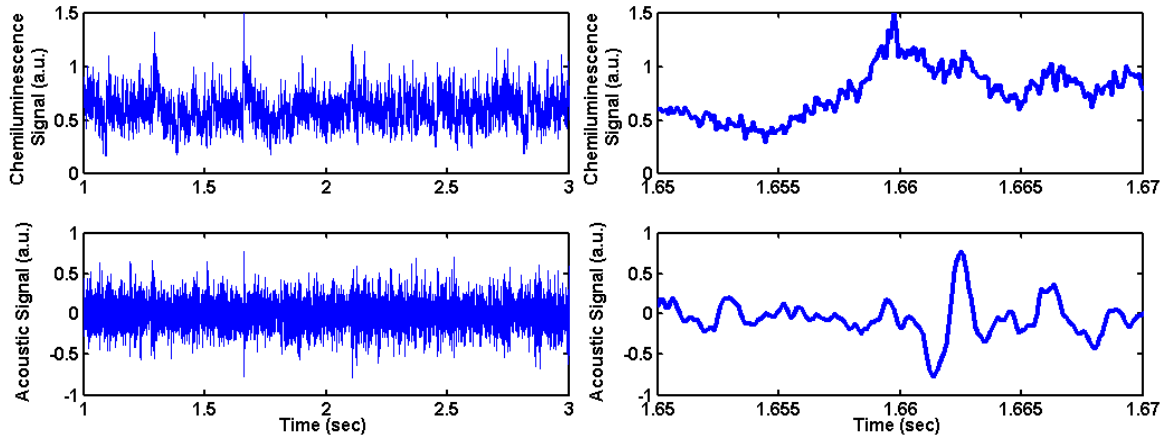

Figure 11 Acoustic and chemiluminescence time series data for ϕ/ϕ_{LBO} = 1.02, close to blowoff (left); and blown-up version of the blowout precursor in the acoustic and optic signal (right).

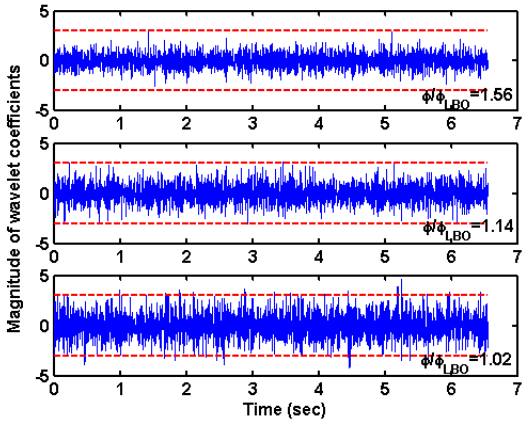

Figure 12 Time dependence of computed $W_2(t)$ wavelet coefficients of acoustic signal at a scale of 36 (~14 Hz) for ϕ/ϕ_{LBO} = 1.56, 1.14 and 1.02.

Figure 12 plots the computed $W_2(t)$ wavelet coefficients at a scale, ψ = 36, roughly corresponding to a frequency of 14 Hz for different normalized equivalence ratios, ϕ/ϕ_{LBO} = 1.56, 1.14 and 1.02. In contrast to the signal R.M.S., see **Figure 6**, the wavelet filtered R.M.S actually increases as the combustor approaches blowout. In addition, large amplitude bursts in the signal ("events") are increasingly obvious.

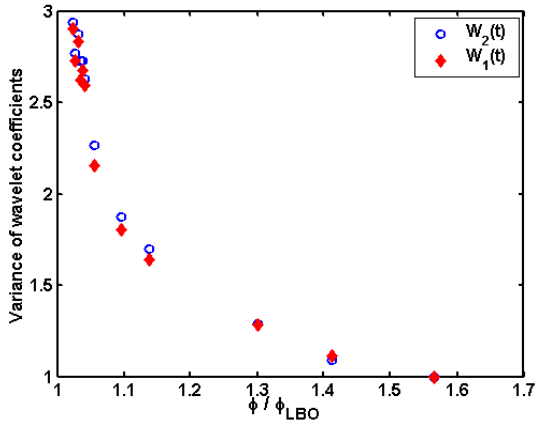

Figure 13 Dependence of $W_2(t)$ and $W_1(t)$ wavelet coefficient variance at scales of 36(~14 Hz) upon ϕ/ϕ_{LBO}.

Figure 13 plots the variance of the wavelet coefficients at a scale, ψ = 36 for $W_1(t)$ and $W_2(t)$ wavelet basis functions. An important point to note is that other wavelet basis functions give very comparable results; i.e., the sensitivity of the change in variance upn basis function is minimal. This can be understood by noting that the wavelet filtering operation is equivalent to streaming the data through a band-pass filter. A straightforward application of Parseval's theorem shows that the variance of the filtered data will be quite similar for a variety of different wavelets, whose Fourier transforms have similar center frequencies and bandwidths. The advantage of identifying a "customized" wavelet lies in its ability to accentuate the amplitude of time-localized events whose shape resembles that of the wavelet, as explained in the next section. As such, the choice of wavelet exerts a large impact upon the statistics of the filtered signal outliers (time-localized events) whose presence we are interested in detecting. As such, the key advantage in customized wavelets lie in using them in conjunction with a discrete event detection algorithm, such as level crossing approaches (discussed in the next section), as opposed to a time-integrated detection algorithm, such as a variance calculation.

Thresholding Approaches

In this section, we discuss the aforementioned level crossing approaches for the acoustic and optic signals. Thresholding the data provides a convenient way of converting a data stream into a quantitative blowout indicator; e.g. a blowoff avoidance logic can be invoked when the data exceeds a threshold level a certain number of times. In the case of the acoustic signal, such techniques were found to be most useful when performed after wavelet filtering. The effect of threshold upon level crossing frequency of the wavelet filtered acoustic signal can be understood from **Figure 14**, which plots the PDF of the $W_2(t)$ wavelet coefficients for ϕ/ϕ_{LBO} = 1.56, 1.14 and 1.02. The increased presence of high amplitude outliers close to blowout results in the long tail in the PDF. The figure indicates that the signal from the stable flames rarely exceeds ~8σ (i.e., 8 times the variance of the $W_2(t)$ coefficients for the stable combustion case).

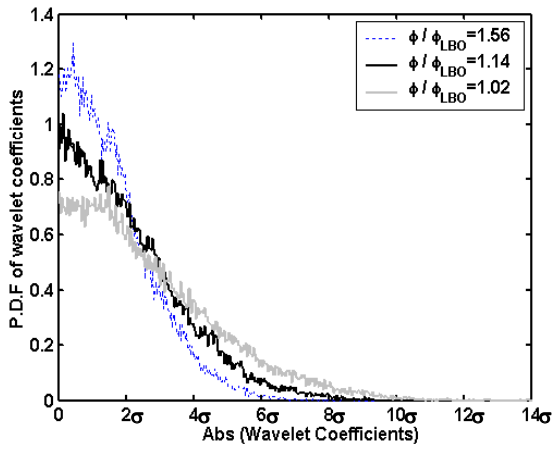

Figure 14 Wavelet transform PDF (using $W_2(t)$) at a scale of 36(~14 Hz) for ϕ/ϕ_{LBO} = 1.56, 1.14 and 1.02,

where σ = the variance of coefficients for the stable combustion case.

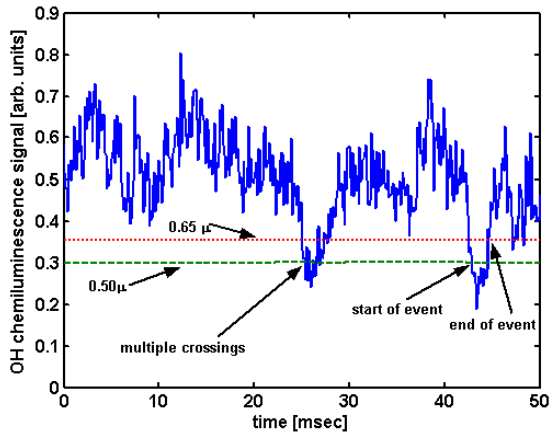

Figure 15 Noise rejection approach based on double thresholding used to detect the blowout precursor events in the chemiluminescence signal.

On the other hand, the optical precursors can be easily identified using a simple thresholding method, where an event is acknowledged when the signal drops below a threshold level. This choice is based on the premise that the precursor signature is initiated by a local extinction event that temporarily lowers the chemiluminescence. Thus the low threshold approach provides the earliest detection of the event. The threshold value was taken to be a fraction of the time-localized mean OH* signal rather than a fixed value. This removes the dependence of the overall signal on power setting variations, and long-term changes in the fiber (e.g., coating) or detector. Here, the local mean signal at a given time is based on the signal averaged over the previous 0.5 seconds. The chemiluminescence signal was found to be very noisy which caused brief increases and drops about the threshold level. To reduce the number of false alarms due to noise in the signal, double thresholding was used (see **Figure 15**). The event starts when the signal drops below a lower threshold, and ends only when the signal goes above the higher threshold. The gap between the two thresholds can be varied based on the noise present in the signal.

Next, we look at the changes in the frequency and duration of such level-crossing events in the acoustic and optic signals close to blowout. **Figure 16** plots the dependence of 9σ level crossing frequency (number of crossings/second) and duration (time the filtered acoustic signal exceeds the threshold/total time) averaged over a period of 6.5 seconds upon ϕ/ϕ_{LBO}. The threshold levels are shown by the dashed lines in **Figure 12**. The number and duration of events rises from identically zero to about 10 events/sec and 20 msec/sec respectively just before blowoff, as seen in **Figure 16**.

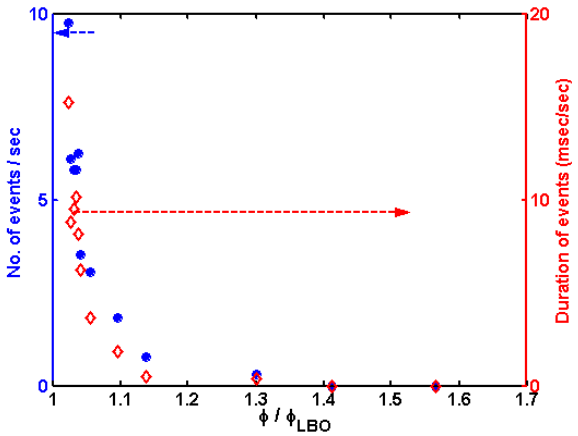

Figure 16 Dependence of the number and duration of acoustic events upon ϕ/ϕ_{LBO}.

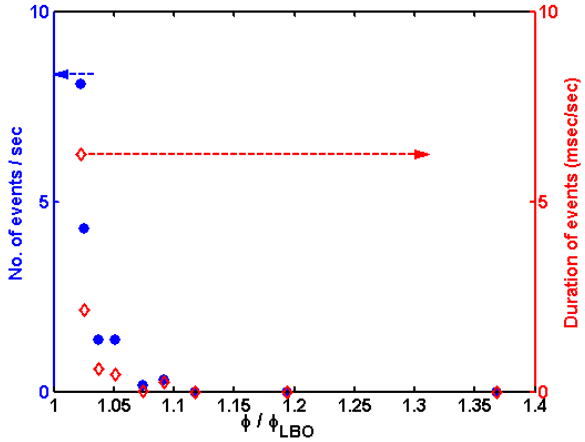

Figure 17 Dependence of the number and duration of chemiluminescence based events upon ϕ/ϕ_{LBO}.

Similarly, **Figure 17** plots the dependence of the number and duration of events in a second (averaged over a period of 6.5 seconds) as blowoff is approached. A lower threshold of 0.50μ was used with the gap between thresholds fixed at 0.15μ. The number and duration of events rises from identically zero to about 8 events/sec and 6 msec/sec respectively just before blowoff, as seen in **Figure 17**. Both parameters behave similarly for both the acoustic and chemiluminescence signal as blowout is approached. Thus either could be used as a blowout proximity measure or a combination

of the two parameters could also be incorporated into a control algorithm for more robustness in detecting blowout.

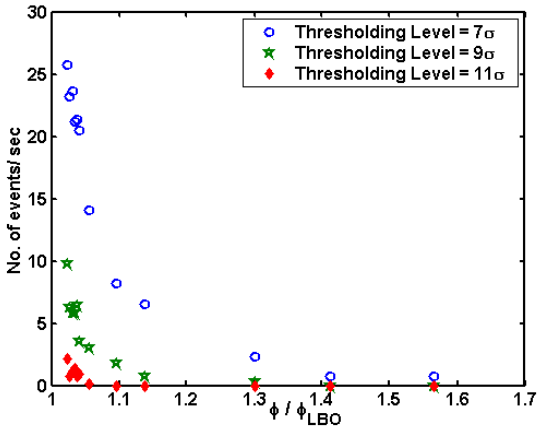

Figure 18 Dependence of the number of acoustic events upon ϕ/ϕ_{LBO} for three thresholding levels, where σ = the variance of coefficients for the stable combustion case.

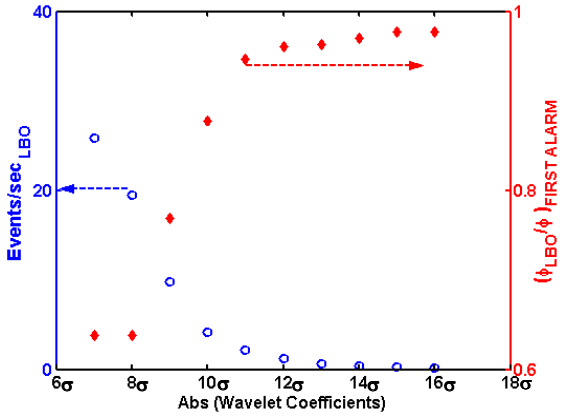

Figure 19 Variation in the number of acoustic events near blowout and the ϕ value where an event is first observed upon thresholding level, where σ = the variance of coefficients for the stable combustion case.

Next, we look at the effect of threshold level on the blowoff proximity measure. **Figure 18** plots the dependence of the number of acoustic events upon ϕ/ϕ_{LBO} at 7σ, 9σ and 11σ thresholds. Note the two influences of the threshold level: number of events detected and the ϕ/ϕ_{LBO} value where events are first detected. With increasing threshold level, there are fewer events detected. Furthermore, no events are detected until the system is very close to blowout. In contrast, at low thresholding levels, the frequency and duration of the alarms close to blowout is much higher, however, events are detected at equivalence ratios much farther from blowout. These tradeoffs in choosing an optimal threshold level are illustrated in **Figure 19**. The left and right y-axes plot the maximum number of events observed before blowoff, and the ϕ value where blowoff is first observed, respectively. As might be anticipated, higher sensitivity results in more alarms at ϕ values where the flame is still reasonably stable. These tradeoffs were alluded to in the discussion of **Figure 8**.

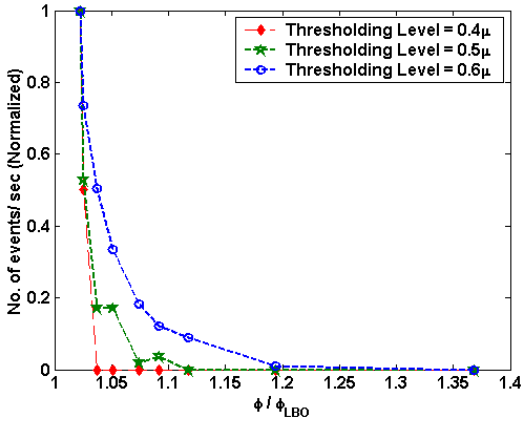

Figure 20 Dependence of the number of chemiluminescence based events upon ϕ/ϕ_{LBO} for three thresholding levels, where μ = the mean of the chemiluminescence signal.

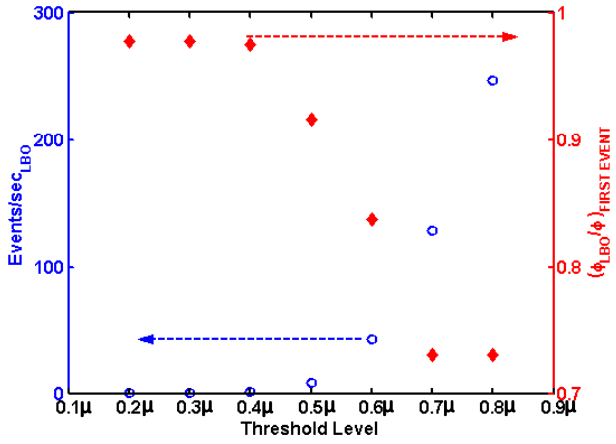

Figure 21 Variation in the number of chemiluminescence based events near blowout and the ϕ value where an event is first observed upon thresholding level, where μ = the mean of the chemiluminescence signal.

Similarly, the effect of threshold level on optic precursors is shown in **Figure 20**, which plots the dependence of the number of events upon ϕ/ϕ_{LBO} at 0.40μ, 0.50μ and 0.60μ thresholds. The values are normalized by their maxima and the curves can be easily compared to that of **Figure 8**. Similar tradeoffs as discussed in the case of the acoustic signal are observed and are quantified in **Figure 21**.

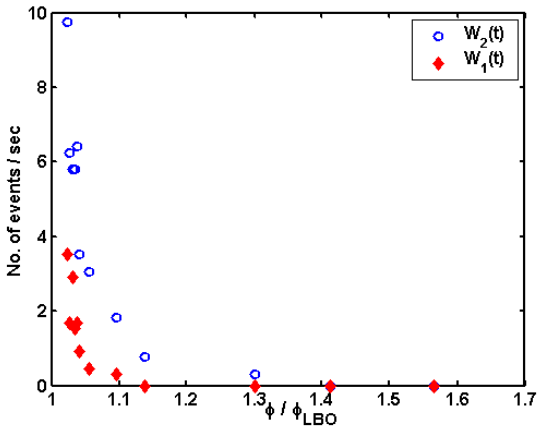

Figure 22 Dependence of the number of events per second upon ϕ/ϕ_{LBO} for two wavelet basis functions in the combustor.

Figure 22 compares the dependence of the number of the crossing frequency upon ϕ/ϕ_{LBO} for the $W_1(t)$ and $W_2(t)$ wavelet basis functions at a scale of 36 (f~14 Hz). Note that the event count of the customized wavelet is almost thrice that of $W_1(t)$. Recall that the choice of the wavelet basis function had little influence upon the variance of the filtered signal (**Figure 13**). This indicates that the sensitivity of the thresholding approach in the acoustic signal is enhanced with the choice of the customized wavelet.

In the case of the optic signal, the threshold approach relied on the change in signal relative to the mean. Therefore, long-term changes in the transmission of the fiber should not be problematic. For example, partial soot deposition on the fiber tip over time would not affect the performance of the sensing technique as long as the signal-to-noise ratio is adequate. Similarly, this method would not be affected by power setting variations during operation of the engine.

Summary and Conclusions

This paper describes an experimental study of the acoustic and chemiluminescence characteristics of pre-mixed flames under near blowoff conditions acquired on a commercial single cup swirl combustor. Near blowout, short time duration, high amplitude bursts in the acoustic signal were observed. These bursts coincided with the occurrence of the flame loss and re-ignition events seen in the high-speed video images. These events were also detected in the OH^* chemiluminescence signal. The precursor events were characterized by brief, often spatially localized, flame extinction events, followed by re-ignition of the unburned fuel/air mixture. These events (both acoustic and optic) increase in frequency and duration as the combustor approaches blowout. An increase in the low frequency regime of the acoustic spectra was also observed which appeared to be controlled by the time interval between events and the duration of the events. Based on the above observations, spectral, wavelet and thresholding based approaches were used to detect precursors to blowoff.

Pronounced changes in the heat release in a localized region of the flame were not very evident in the overall acoustic signal as it was a spatially integrated measure of the unsteady heat release over the entire flame. Thresholding techniques were found to be most useful when performed after wavelet filtering of the acoustic data. In contrast, because optical measurements could be focused upon localized spatial regions, thresholding of the raw signal was easy to implement. The number and duration of precursor events were found to increase from identically zero to about 10 events/sec and 20 msec/sec respectively in case of the acoustic signal, and to about 8 events/sec and 6 msec/sec respectively in the chemiluminescence signal just before blowoff. The choice of threshold level had a substantial effect on the sensitivity of the blowout proximity indicator and could be optimized for a given combustor. Further studies are underway to understand the nature and evolution of the precursor events in high-pressure combustors.

Acknowledgements

This research was supported by the GE Aircraft Engines (Dr. Tim Held and Dr. Hukam Mongia, technical monitors), National Science Foundation (Dr. Farley Fisher, technical monitor), NASA Ames (Dr. L. S. Fletcher, technical monitor), and the US Department of Energy, Office of Fossil Energy, National Energy Technology Laboratory (Dr. Richard Wenglarz, technical monitor).

References

[1] Rosfjord, T. J. and Cohen, J. M., "Evaluation of the Transient Operation of Advanced Gas Turbine Combustors", *Journal of Propulsion and Power*, Vol.11 (3), 1995, pp. 497-504.

[2] Nair, S., and Lieuwen, T., "Acoustic Characterization of Premixed Flames under Near Blowout Conditions", *AIAA Paper 2002-4011*, 38th AIAA Joint Propulsion Conference, July 2002.

[3] Nair, S., and Lieuwen, T., "Acoustic Detection Of Imminent Blowout In Pilot And Swirl Stabilized Combustors", *ASME Paper 2003-38074*, ASME-IGTI Turbo Expo Conference, June 2003.

[4] Nair, S., and Lieuwen, T., "Acoustic Emissions of Premixed Flames In Swirl And Bluff Body Stabilized Combustors Near Flameout", *AIAA Paper 2003-5084*, 39th AIAA Joint Propulsion Conference, July 2003.

[5] Muruganandam, T. M., Nair, S., Neumeier, Y., Lieuwen, T.C., Seitzman, J.M., "Optical And Acoustic Sensing Of Lean Blowout Precursors", *AIAA Paper 2002-3732*, 38th AIAA Joint Propulsion Conference, July 2002.

[6] Sturgess, G., "Lean Blowout in a Research Combustor at Simulated Low Pressures", *ASME paper 91-GT-359*, 1991.

[7] Nicholson, H., Field, J., "Some Experimental Techniques for the Investigation of the Mechanism of Flame Stabilization in the Wake of Bluff Bodies", *Proc. Comb. Inst.*, Vol.3, 1951, pp. 44-68.

[8] Chao, Y.C., Chang, Y.L., Wu, C.Y., Cheng, T.S., "An Experimental Investigation of the Blowout Process of a Jet Flame," *Proc. Comb. Inst.*, Vol.28, 2000, pp. 335-342.

[9] Hedman, P.O., Fletcher, T.H., Graham, S.G., Timothy, G.W., Flores, D.V., and Haslam, J.K., "Observations of Flame Behavior in a Laboratory-Scale Pre-mixed Natural Gas/Air Gas Turbine Combustor from PLIF measurements of OH", *ASME Paper* GT-2002-30052, *Proceedings of ASME TURBO EXPO*, 2002.

[10] Wohl, K., Kapp, N.M., and Gazley, C., "Flame Stabilization and Quenching", *Proc. Comb. Inst.*, Vol.3, 1951, pp. 3-21.

[11] Longwell, J.P., Chenevey, J., Clark, W., and Frost, E., "Flame Stabilization by Baffles in a High Velocity Gas Stream", *Proc. Comb. Inst.*, Vol.3, 1951, pp. 40-44.

[12] Williams, G., Hottel, H., Scurlock, A., "Flame Stabilization and Propagation in High Velocity Gas Streams", *Proc. Comb. Inst.*, Vol.3, 1951, pp. 21-40.

[13] Jensen, W.P., Shipman, C.W., "Stabilization of Flames in High Speed Flows By Pilot Flames", *Proc. Comb. Inst.*, Vol.7, 1951, pp. 674-680.

[14] Williams, G.C., Shipman, C.W., "Some Properties of Rod Stabilized Flames of Homogeneous Gas Mixtures", *Proc. Comb. Inst.*, Vol.4, 1953, pp. 733-742.

[15] Petela, G., Petela, R., "Diagnostic Possibilities on the Basis of Premixed Flame Noise Levels", *Comb. Flame*, Vol. 52, 1983, pp. 137-147.

[16] Gaydon, A.G. and Wolfhard, H.G., "*Flames: Their Structure, Radiation, and Temperature*", Fourth edition, Chapman and Hall, 1978.

[17] Keller, J.O. and Saito, K., "Measurements of the Combusting Flow in a Pulse Combustor", *Combustion Science and Technology*, Vol. 53, 1987, pp. 137-163.

[18] Lawn, C.J., "Distributions of Instantaneous Heat Release by the Cross-Correlation of Chemiluminescent Emissions," *Combustion and Flame*, Vol. 132, 2000, pp. 227-240.

[19] Roby, R.J., Hamer, A.J., Johnsson, E.L., Tilstra, S.A., and Burt, T.J., "Improved Method for Flame Detection in Combustion Turbines", *Transactions of the ASME*, Vol. 117, 1995, pp. 332 –340.

[20] Mehta, G.K., Ramachandra, M.K., and Strahle, W.C., "Correlations between Light Emission, Acoustic Emission and Ion Density in Premixed Turbulent Flames", *Proc. Comb. Inst.*, Vol.18, 1981, pp 1051-1059.

[21] Najm, H. N., Paul, P.H., Mueller, C. J., and Wyckoff, P. S., "On adequacy of certain experimental observables as measurements of flame burning rate", *Comb. Flame*, Vol. 113, pp 312-332.

[22] Khanna,V. K., Vandsburger, U., Saunders W. R., Baumann, W. T., "Dynamic analysis of swirl stabilized turbulent gaseous flames", *ASME Paper GT-2002-30061*, Proceedings of ASME Turbo Expo, 2002.

[23] Ikeda, Y., Kojima, J., Nakajima, T., "Local Damkohler number measurement in turbulent methane/air premixed flames by local OH^*, CH^* and C_2^* chemiluminescence", *AIAA Paper 2000-3395*, 36th AIAA/ASME/SAE/ASEE Joint Propulsion Conference, 2000.

[24] Groechnig, K., "*Foundations of Time-Frequency Analysis*", Birkhaeuser, Boston, 2000.